Chemical Engineering Journal 228 (2013) 834–842

Contents lists available at SciVerse ScienceDirect

Chemical Engineering Journal

journal homepage: www.elsevier.com/locate/cej

Synthesis of TiO_2 hollow sphere multimer photocatalyst by etching titanium plate and its application to the photocatalytic decomposition of gaseous styrene

Jiangyao Chen [a,b], Xin Nie [a,b], Huixian Shi [a], Guiying Li [a], Taicheng An [a,*]

[a] State Key Laboratory of Organic Geochemistry, Guangdong Key Laboratory of Environmental Resources Utilization and Protection, Guangzhou Institute of Geochemistry, Chinese Academy of Sciences, Guangzhou 510640, PR China
[b] University of Chinese Academy of Sciences, Beijing 100049, PR China

HIGHLIGHTS

- TiO_2 hollow sphere multimer was obtained by etching Ti plate in NH_4F solution.
- The photocatalysts showed better degradation ability to gaseous styrene than P25.
- Formation process includes multimer formed on Ti plate and hollowed in solution.

GRAPHICAL ABSTRACT

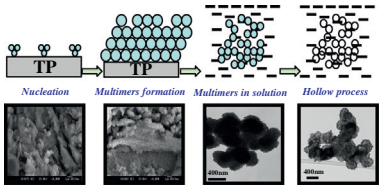

ARTICLE INFO

Article history:
Received 27 February 2013
Received in revised form 13 May 2013
Accepted 16 May 2013
Available online 25 May 2013

Keywords:
TiO_2 hollow sphere multimer
Photocatalyst
Volatile organic compounds
Decomposition
Formation mechanism

ABSTRACT

TiO_2 hollow sphere multimer photocatalyst (SPMP) was synthesized by a one-step hydrothermal method using titanium plate (TP) as the titanium source and NH_4F as the structure regulator. The structural properties of prepared photocatalysts were characterized using X-ray diffraction, UV–vis absorption spectra, N_2 adsorption–desorption, scanning electron microscopy and transmission electron microscopy. The results indicated that the additional amount of NH_4F and hydrothermal time played significant roles in the formation of the TiO_2 SPMP. TiO_2 SPMP could be obtained only when 0.80 g NH_4F as well as TP were added to 40 mL of deionized water and then hydrothermally treated for 22 h at 120 °C. The photocatalytic activity of multimer photocatalysts fabricated under various conditions was evaluated and optimized to decompose gaseous styrene. The results revealed that all prepared photocatalysts (hollow or solid sphere multimers) showed better photocatalytic activity than Degussa P25 in the decomposition of gaseous styrene. TiO_2 SPMP displayed the highest photocatalytic activity due to the synergistic effects of its large surface area, good anatase crystallinity, and unique hollow multimer structure as well as its relatively wide band energy. A preliminary two-major-step formation mechanism for hollow sphere multimers was proposed: The multimers were formed on the TP, followed by a hollowing process for multimers in the solution.

1. Introduction

In the past few decades, heterogeneous photocatalysis has been attracting much attention because it is a green technology that can potentially be applied to environmental remediation [1–4]. Photocatalysis plays an important role in this process. To date, TiO_2 has been used as the dominant photocatalyst to remove organic pollutants due to its properties of superior photocatalytic oxidation ability, nonphotocorrosiveness, chemical inertness and inexpensive characteristics [5–9]. Some inherent drawbacks, such as small specific surface area and low adsorption capability [10–13], still exist for conventional TiO_2 in practical environmental cleaning applications. Because heterogeneous photocatalysis is a

* Corresponding author. Address: State Key Laboratory of Organic Geochemistry, Guangzhou Institute of Geochemistry, Chinese Academy of Sciences, No. 511 Kehua Street, Tianhe District, Guangzhou, Guangdong 510640, PR China. Tel.: +86 20 85291501; fax: +86 20 85290706.
E-mail address: antc99@gig.ac.cn (T. An).

1385-8947/$ - see front matter © 2013 Elsevier B.V. All rights reserved.
http://dx.doi.org/10.1016/j.cej.2013.05.066

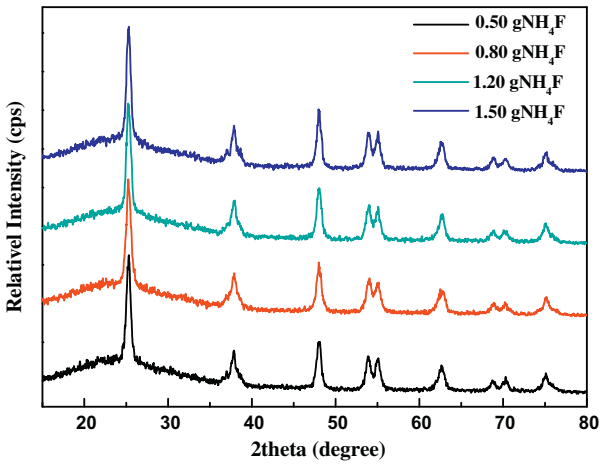

Fig. 1. XRD patterns of power photocatalysts obtained with the addition of different amounts of NH_4F.

surface-mediated advanced oxidation process and photocatalysts with higher surface areas can enhance mass transfer of pollutants to its surface, the photonic efficiency of the photocatalyst can also be improved by an increase in the surface exposure to photons [14]. The synthesis of TiO_2 with high surface area is therefore very necessary for its practical application to harvest more pollutants as well as light.

Since Honda and Fujishima first discovered the photocatalytic splitting of water on TiO_2 electrodes in 1972 [15], TiO_2 photocatalysts with various morphologies and performances have been explored in the past few decades. The TiO_2 hollow sphere photocatalyst has attracted considerable attention due to its high surface area, high porosity, low bulk density, great light-harvesting capacity, and higher photocatalytic activity for pollutants than the TiO_2 particle photocatalyst [16–18]. To fabricate TiO_2 hollow sphere photocatalysts, hard or soft templates such as polystyrene beads [19,20], carbonaceous materials [21–23] and surfactants [24] have frequently been used to hydrolyze titanium precursors. The templates were then removed by subsequent calcination or dissolution processes. However, the preparation procedure with a template is always complex, and the properties of the resultant hollow or porous materials depend significantly on the nature and concentration of the template. A template-free method for

Table 1
Effect of the amount of NH_4F on structural properties of powder photocatalysts.

Amount of NH_4F (g)	Crystalline size (nm)	BET[a] surface area ($m^2\ g^{-1}$)	Average pore size (nm)	BJH[b] total pore volume ($cm^3\ g^{-1}$)	Relative crystallinity[c]
0.50	15.0	101.1	11.9	0.380	1.00
0.80	15.9	70.5	17.9	0.373	1.18
1.20	16.5	68.4	16.9	0.331	1.20
1.50	17.1	67.6	16.5	0.323	1.22

[a] Brunauer–Emmett–Teller.
[b] Barrett–Joyner–Halen.
[c] The relative intensity of the diffraction peak from the anatase (101) plane (reference = the sample prepared with the amount of 0.50 g NH_4F).

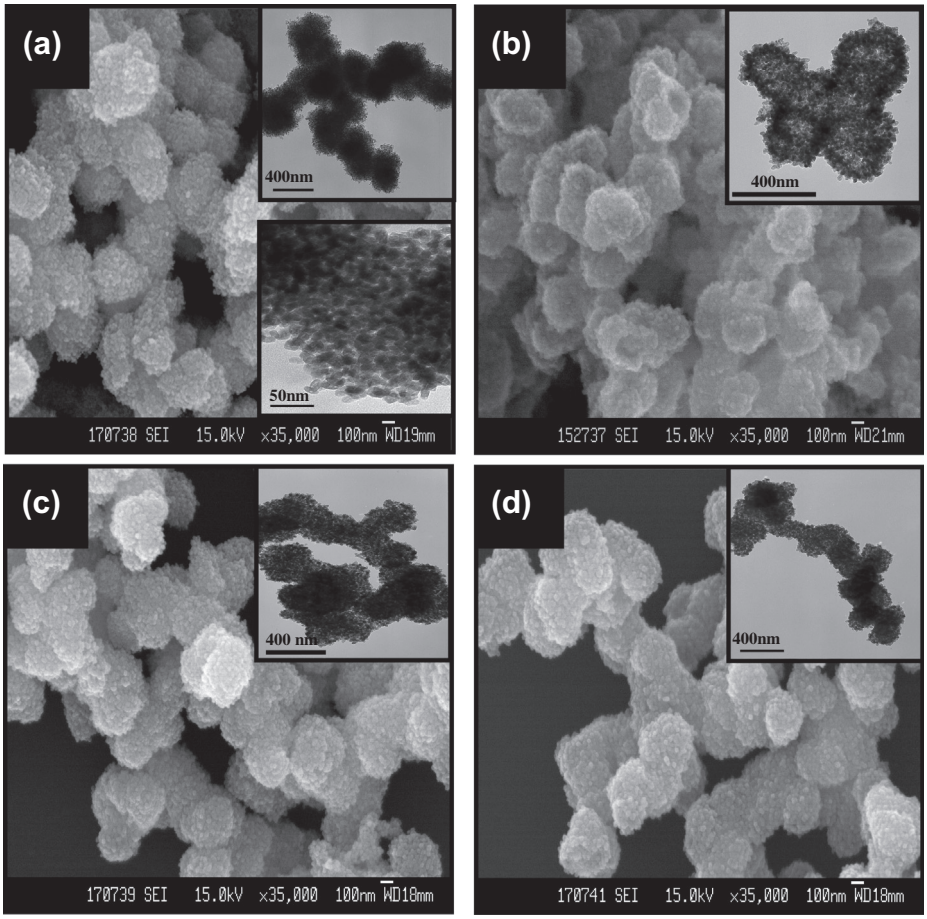

Fig. 2. SEM and TEM images of power photocatalysts prepared with addition of different amounts of NH_4F ((a) 0.50 g; (b) 0.80 g; (c) 1.20 g; (d) 1.50 g).

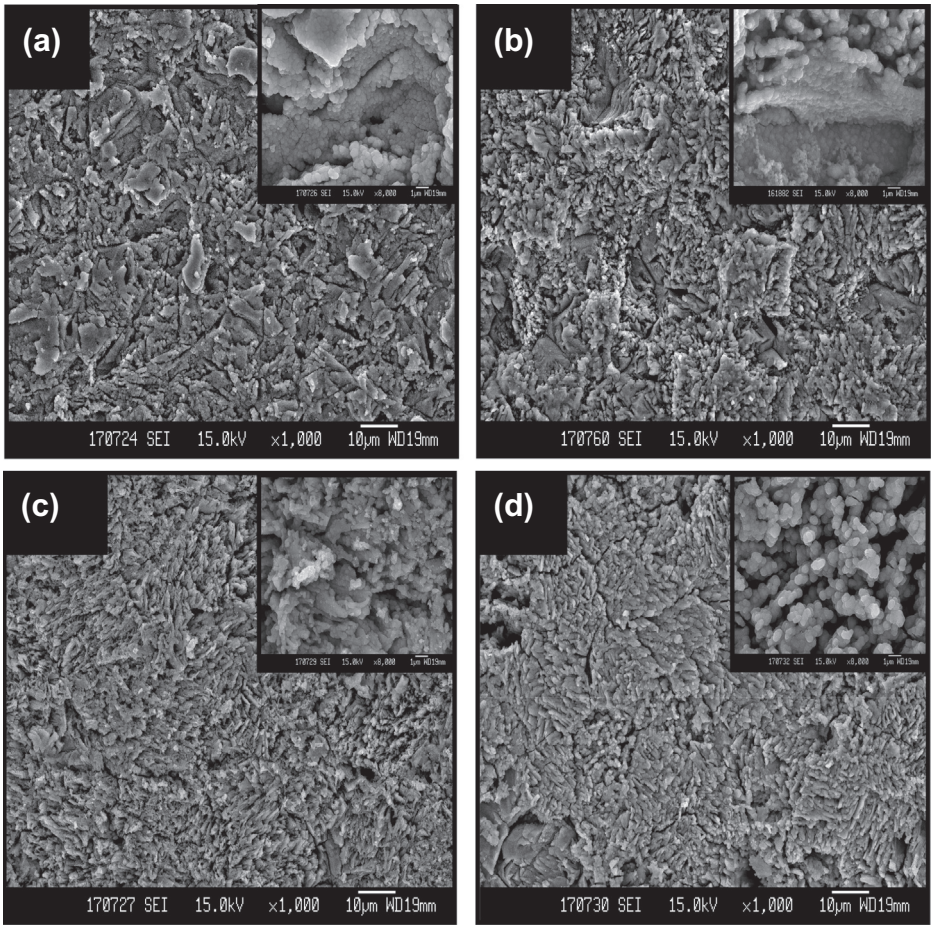

Fig. 3. SEM images of the TP after hydrothermal reaction with addition of different amounts of NH_4F ((a) 0.50 g; (b) 0.80 g; (c) 1.20 g; (d) 1.50 g).

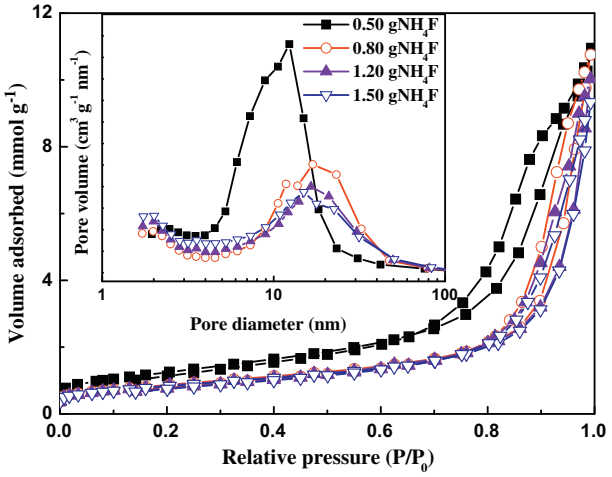

Fig. 4. N_2 adsorption–desorption isotherms and corresponding pore size distribution curves for powder photocatalysts obtained with the addition of different amounts of NH_4F.

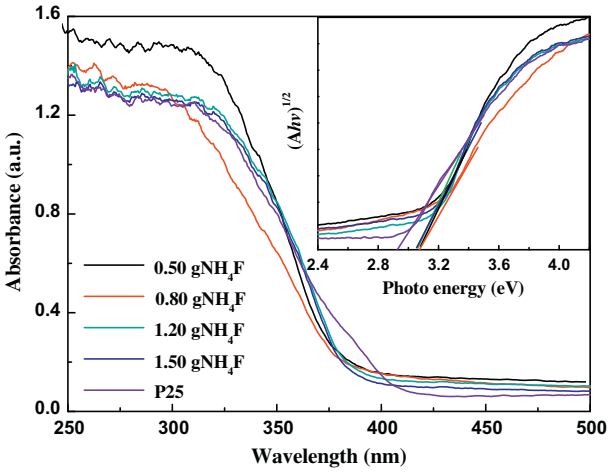

Fig. 5. UV–vis absorption spectra of P25 and the powder photocatalysts obtained with the addition of different amounts of NH_4F.

direct synthesis of a TiO_2 hollow sphere photocatalyst is preferred in practical applications due to the ease of handling and scaling up. TiO_2 hollow spheres have been fabricated by direct hydrothermal treatment of mixed $Ti(SO_4)_2$, NH_4F and H_2O [6,17]. Unfortunately, due to the swift and intense reaction caused by the relatively high reaction temperature (higher than 160 °C), a large number of small particles can also be observed in the reaction products in addition to hollow spheres. Recently, some researchers attempted to solve this problem by using titanium powder as the starting material [25]. Although very few free particles were obtained, the coexistence of unreacted titanium powder could subsequently influence the photocatalytic activity of the prepared samples. To overcome this problem, titanium plate (TP) was used as an alternative for

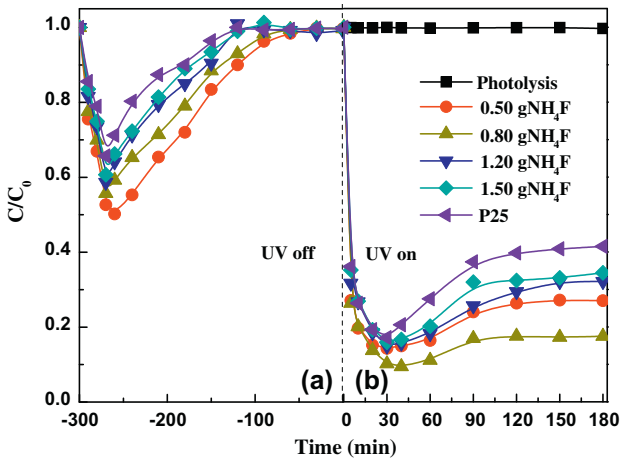

Fig. 6. Adsorption, photolysis and photocatalytic decomposition kinetic curves of styrene by P25 and the powder photocatalysts prepared with addition of different amounts of NH_4F.

the synthesis of TiO_2 spheres on the TP directly by the hydrothermal method to eliminate the need for separation of the titanium precursor from the resultant photocatalyst [26]. However, the authors in this study focused only on the fabrication and characterization of the TP electrode, while the formation mechanism and application of the sample powder falling from the TP were completely ignored. By successfully controlling the reaction parameters, well-defined TiO_2 hollow sphere multimer photocatalyst (SPMP) with both high adsorption capability and photocatalytic activity can easily be fabricated. Nevertheless, to the best of our knowledge, the synthesis of TiO_2 hollow sphere multimers through the direct corrosion of TP by a hydrothermal method has not yet been described in the published literature.

This work therefore reports that a TiO_2 hollow sphere multimer was directly synthesized for the first time by hydrothermal etching TP using NH_4F as the structure regulator. The effects of additional amounts of NH_4F and variation of hydrothermal time were investigated in detail, and the adsorption ability as well as the photocatalytic activity of the prepared samples was evaluated in a continuous flow-through reactor by selecting gaseous styrene as the model organic pollutant. Finally, a formation mechanism was also proposed.

2. Experimental methods

2.1. Synthesis of photocatalysts

TP (1.5 cm × 1.5 cm × 0.16 mm, 99.6% purity, Baoji Haiji Titanium & Nickel Co., Ltd., China) was sonically degreased sequentially with acetone (15 min), 2-propanol (15 min), methanol (15 min) and then deionized water, followed by drying in an oven.

For a typical synthetic process of the TiO_2 (SPMP), 0.80 g NH_4F was first dissolved in 40 mL deionized water by stirring to obtain a transparent solution. A piece of pretreated TP was then added to the solution, and the solution was then hydrothermally treated in an autoclave at 120 °C for 22 h. The wet precipitate and TP were subsequently collected, washed thoroughly with distilled water and ethanol, dried at 80 °C for 8 h, and finally calcined at 500 °C for 2 h.

2.2. Characterization of structure and morphology

X-ray diffraction (XRD) patterns were recorded on a Rigaku Dmax X-ray diffractometer. The ultraviolet–vis (UV–vis) absorption spectra were obtained with a UV–vis spectrophotometer (UV-2501PC). Nitrogen adsorption–desorption isotherms were obtained with a Micromeritics ASAP 2020 system. Image and microstructure data for the prepared samples were acquired with scanning electron microscopy (SEM, JSM-6330F) and transmission electron microscopy (TEM, JEM100CX).

2.3. Characterization of adsorption ability and photocatalytic activity

The adsorption ability and photocatalytic activity of the prepared photocatalysts were evaluated using gaseous styrene (initial concentration of 15 ± 1 ppmv) as a model volatile organic compound (VOC) in a continuous flow mode [27]. And the diagram of the experimental set-up is shown in Fig. S1. In a typical experimental process, 0.10 g of prepared photocatalyst powder was loaded into a cubic quartz glass reactor (1.0 cm × 1.0 cm × 0.5 cm). A 365 nm UV-LED spot lamp (Shenzhen Lamplic Science Co., Ltd.) was used as a light source fixed vertically on top of the reactor at a distance of 6 cm (the UV intensity was controlled at 70 mW cm^{-2}). Before the lamp was switched on, the pollutant was allowed to reach gas–solid adsorption equilibrium. The concentrations of pollutant were analyzed by a gas chromatograph (GC-900A) equipped with a flame ionization detector. The temperatures of the column, injector and detector were 110, 230 and 230 °C, respectively. Gas samples were collected at regular intervals using a gas-tight locking syringe (Agilent, Australia), and a 200 μL gas sample was injected into the column in splitless mode for determination of concentration.

The adsorption efficiency and photocatalytic degradation efficiency were both calculated for styrene according to the following equation.

$$\text{Efficiency} = (1 - C/C_0) \times 100\% \quad (1)$$

where C is the concentration of residual pollutant, and C_0 is its original concentration.

3. Results and discussion

3.1. XRD pattern analysis

The wide angle XRD patterns of the prepared photocatalysts obtained with different added amounts of NH_4F are shown in Fig. 1. Only characteristic peaks of anatase TiO_2 at 2θ = 25.3, 37.2, 48.9, 54.0, 55.3 and 62.4° are observed in the XRD patterns, indicating that anatase TiO_2 is the only crystalline phase in all of the prepared photocatalysts. In addition, the crystalline size of the resultant samples are calculated from the broadening of the XRD peak at 2θ = 25.3° according to the Scherrer formula (Table 1). Results indicated that, although the corresponding characteristic peaks at 2θ = 25.3° seem no obvious change, the size of crystalline TiO_2 increased for samples obtained with the increase of the amount of NH_4F addition. When 0.50 g NH_4F is added to the solution, the crystalline size of TiO_2 in the resultant photocatalyst is calculated as 15.0 nm. The size increased to 15.9, 16.5 and 17.1 nm when the added amount of NH_4F was increased to 0.80, 1.20 and 1.50 g, respectively. In addition to the increase of the crystalline size of TiO_2, the relative crystallinity of the photocatalyst also increased from 1.00 to 1.22 with the increase in the amount of NH_4F added from 0.50 to 1.50 g. The possible reason may be that F^- can enhance the crystallization of the anatase phase and accelerate the growth of crystals [18]. Similar results can also be obtained from previous reports [6,28].

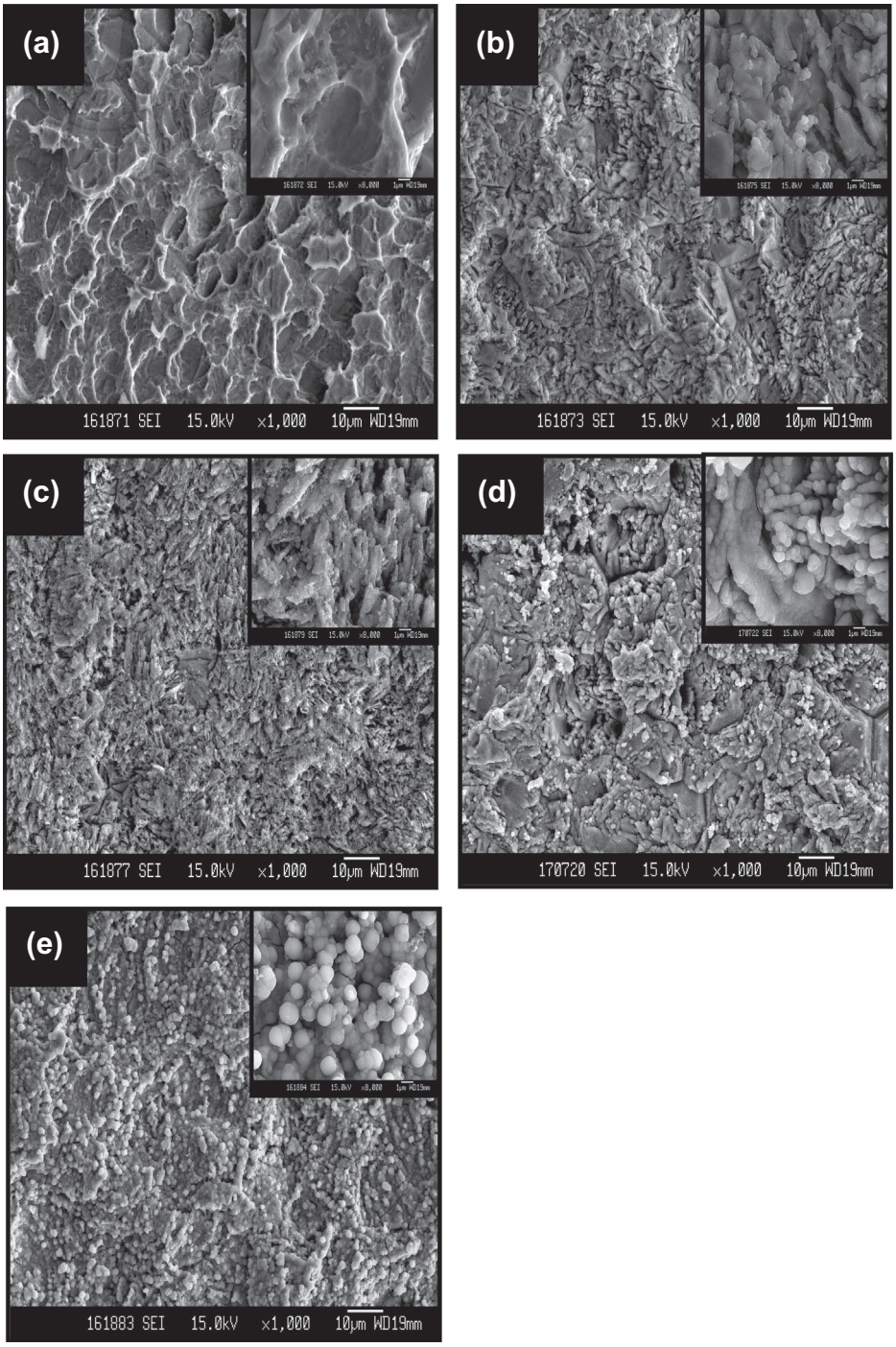

Fig. 7. SEM images of the TP after reaction with 0.80 g NH_4F at different hydrothermal times ((a) 2 h; (b) 6 h; (c) 12 h; (d) 36 h; (e) 48 h).

3.2. SEM and TEM image analysis

To investigate the effect of the added amount of NH_4F on the resultant photocatalysts, their morphology and microstructure were examined by SEM and TEM. Fig. 2 shows that the photocatalyst obtained with the added amount of 0.50 g NH_4F consists of solid TiO_2 spheres with an average diameter of approximately 400 nm, and this diameter remained basically unchanged with an increase in the added amount of NH_4F to 1.50 g. The effect of NH_4F on the sphere size appeared to be negligible. Further observation indicated that the TiO_2 spheres were connected to each other to form multimers. This formation of multimers may occur because of the existence of the Ti–OH group on the surface of the spheres [6]. The surface of the spheres was very rough, and the TEM image (inset of Fig. 2a) indicated that the spheres were composed of nanoparticles with an average diameter of approximately 15 nm. This result was consistent with the result of the XRD pattern analysis. With the increase of the added amount of NH_4F to 0.80 g (Fig. 2b), more sphere multimers with open holes could be discerned, and the TEM image (inset of Fig. 2b) confirmed that the resultant photocatalyst was composed of multimeric TiO_2 hollow spheres. Increasing the added amount of NH_4F further to 1.20 (Fig. 2c) and 1.50 g (Fig. 2d) resulted in solid sphere multimers being found in the photocatalysts obtained. These results

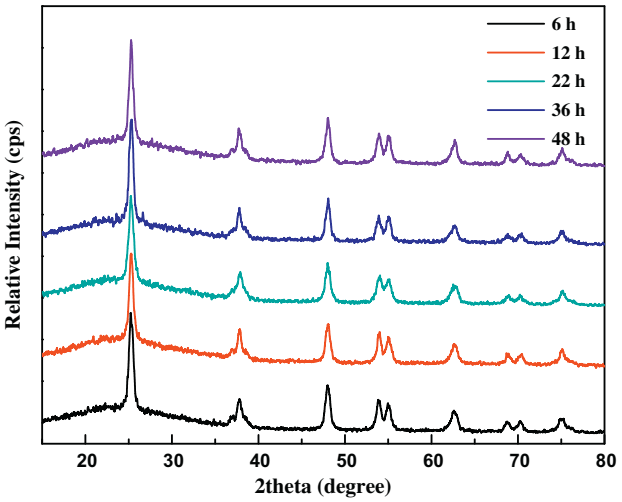

Fig. 8. XRD patterns of the powder after reaction with 0.80 g NH_4F at different hydrothermal times.

suggested that the formation of hollow sphere multimers was very closely dependent on the amount of NH_4F added during the preparation process, and the TiO_2 (SPMP) could be synthesized exactly only when the added amount of NH_4F was selected as 0.80 g in this study.

In addition to examination of the resultant photocatalysts precipitating from the solution, the effect of the added amount of NH_4F on the morphology change of the corresponding TPs was also examined by SEM (Fig. 3 and Fig. S2). From Fig. S2, it can be seen that the raw TP is very flat and no particles can be observed on the TP. As shown in Fig. 3a, with the added amount of 0.50 g NH_4F, the surface of the TP became rough, and a number of independent massive particles were formed. Further observation from the inset of Fig. 3a showed that these massive particles were composed of multilayered spherical particles, and they were connected closely with each other. The average diameter of each particle was approximately 400 nm, consistent with the particle size in the corresponding powder sample. When the added amount of NH_4F was increased to 0.80 g, the TP was etched further, and its surface became rougher (Fig. 3b). In addition to multilayered spherical particles, more relatively independent particle multimers were observed (inset of Fig. 3b). When the added amount of NH_4F was further increased to 1.20 (Fig. 3c) and 1.50 g (Fig. 3d), the TP surface became rougher and rougher and was almost covered by independent particle multimers. Comparing the SEM images shown in Figs. 2 and 3, particles on the TP and in its corresponding powder sample were found to possess similar morphology and size, although the surface of the particles in the powder sample was much rougher. All these observations suggest that the TiO_2 particles in the powder sample originated directly from TP etching, then underwent a growth process in the TiO_2 crystals, and finally formed spherical multimers with or without a hollowing process.

3.3. N_2 adsorption–desorption isotherm analysis

Fig. 4 shows the N_2 adsorption–desorption isotherms of the prepared powder photocatalysts obtained with the different added amounts of NH_4F. All samples showed similar type IV isotherms (IUPAC classification) with the same typical H3 hysteresis loops, indicating the existence of mesoporous structures and slit-like pores [29]. The average pore size of the sample prepared with 0.50 g NH_4F added was calculated as 11.9 nm, which increased to 17.9 nm with the increase in the amount of NH_4F added to 0.80 g and decreased slightly to 16.9 and 16.5 nm as the added amount of NH_4F increased continuously to 1.20 and 1.50 g (the inset of Fig. 4). These prepared samples were obviously all mesoporous materials. The quantitative details about the Brunauer–Emmett–Teller (BET) surface areas, Barrett–Joyner–Halen (BJH) total pore volumes and average pore diameter are also listed in Table 1. Increasing the added amount of NH_4F from 0.50 to 1.50 g, both BET surface area and total pore volume of the samples decreased from 101.1 $m^2 g^{-1}$ and 0.380 $cm^3 g^{-1}$ to 67.6 $m^2 g^{-1}$ and 0.323 $cm^3 g^{-1}$. Similar result is also obtained by Yu et al. due to the increase of crystalline sizes and disappearance of some small pores [18]. Moreover, the BET surface areas of all prepared samples in this study are higher than that of P25 (surface area of 50 m^2/g). Larger BET surface area and bigger total pore volume might lead to higher adsorption capacity for gaseous organic pollutants, which will be verified by the following adsorption experiments.

3.4. UV–vis spectral analysis

Fig. 5 shows the UV–vis absorption spectra and the indirect band energy of the prepared powder photocatalysts as well as P25. All samples exhibited the typical absorption with an intense transition in the UV region of the spectrum, which was attributed to the electron transition of TiO_2 from the valence band to the conduction band [30]. Compared with P25, the obvious blue shift in the absorption edge of the spectra of all prepared powder photocatalysts was observed, which might be a result of the quantum-size effect from the smaller average crystalline size of the porous TiO_2 hollow aggregates [17]. This result is consistent with the crystalline size for prepared samples (15.0–17.1 nm) and P25 (25 nm). The indirect band gap energies of the prepared powder photocatalysts and P25 could be estimated from a plot of $(\alpha h\nu)^{1/2}$ versus photon energy ($h\nu$) (inset in Fig. 5). The intercept of the tangent to the plot gave a good approximation of the indirect band gap energy for TiO_2 [31]. The absorption coefficient α could be calculated from the absorbance [32,33]. From the inset in Fig. 5, the indirect band gap energies estimated from the intercept of the tangents to the plots are 3.06, 3.07, 3.09 and 3.10 eV for the prepared powder photocatalysts obtained with the added amounts of 0.50, 0.80, 1.20 and 1.50 g NH_4F, respectively, which are all higher than P25 (2.97 eV).

3.5. Adsorption and photocatalytic decomposition performance with gaseous styrene

To evaluate the adsorption capability and photocatalytic activity of the prepared photocatalysts, gaseous styrene was selected as a model VOC. Fig. 6 shows the adsorption, direct photolysis and photocatalytic decomposition curves of styrene for P25 as well as synthesized powder photocatalysts prepared with the different amounts of additional NH_4F.

Before switching on the lamp, the adsorption equilibrium experiments were first conducted (Fig. 6a). From the figure, styrene was adsorbed swiftly onto all samples during the initial 20–30 min until slow breakthrough occurred (breakthrough point is defined here where the outlet concentration of styrene is equal to 5% of the inlet styrene concentration). For P25 and the photocatalysts prepared with the added amounts of 1.20 and 1.50 g NH_4F, the complete breakthrough (when the outlet and inlet concentrations of styrene are equal) was observed only after 180 min of adsorption, suggesting that the adsorption capabilities of these three samples for styrene were relatively poor. The times for complete breakthrough were apparently extended to 270 and 240 min for the samples prepared with the added amounts of 0.50 and 0.80 g NH_4F. The time for complete breakthrough clearly follows the order: 1.50 g NH_4F = 1.20 g NH_4F = P25 < 0.80 g NH_4F < 0.50 g NH_4F,

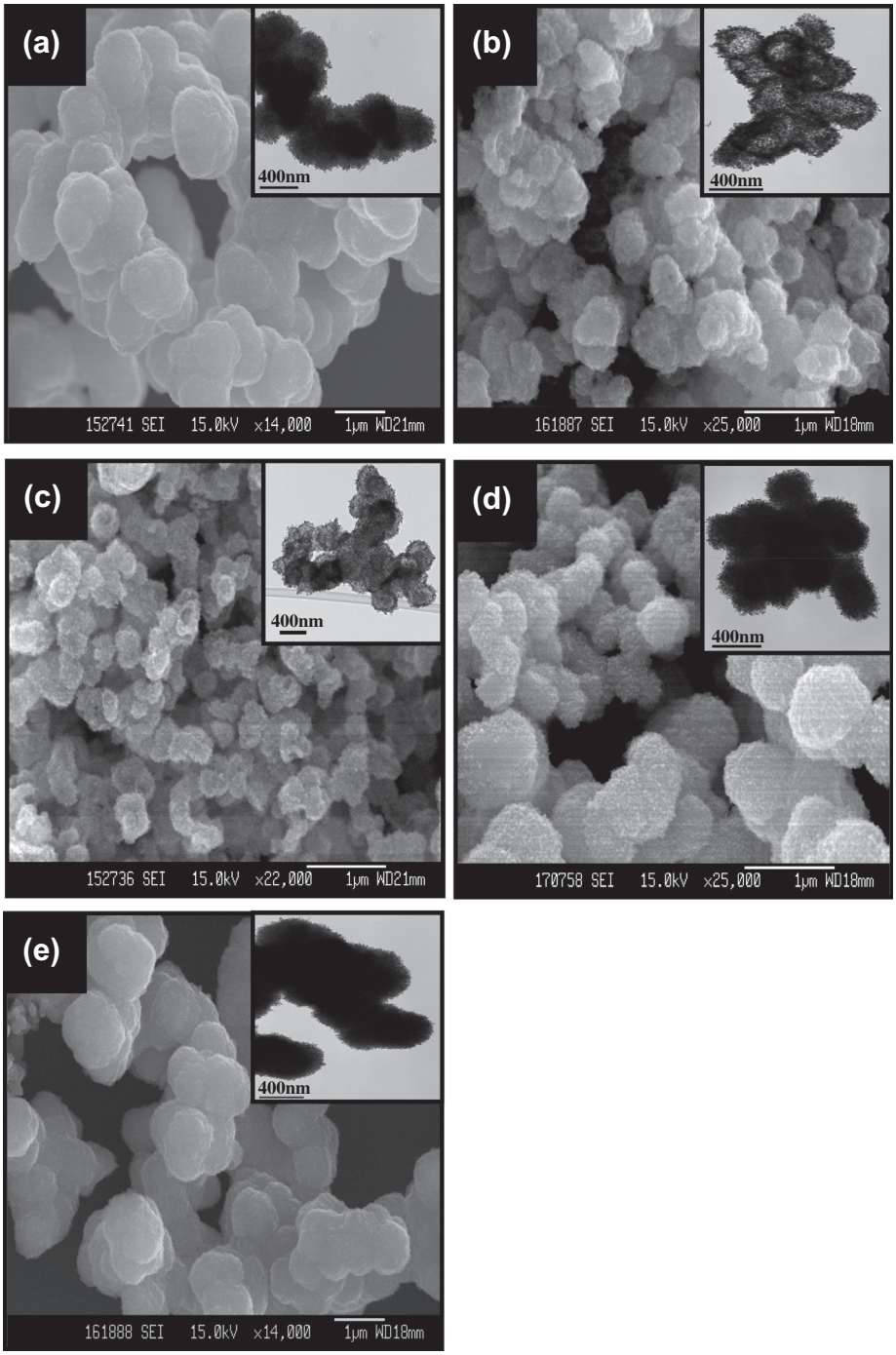

Fig. 9. SEM and TEM images of the powder photocatalysts after reaction with 0.80 g NH_4F at different hydrothermal times ((a) 6 h; (b) 12 h; (c) 22 h; (d) 36 h; (e) 48 h).

consistent with the results from determination of BET surface area and BJH total pore volume. The sample with the larger surface area and bigger total pore volume possesses higher adsorption capacity for VOCs in this work.

When the adsorption reaches equilibrium, the lamp is switched on (Fig. 6b). First, the control experiment of direct photolysis was also carried out, and less than 1% of the styrene was removed after 180 min of photolysis, indicating that UV light only cannot efficiently decompose the styrene. For P25 (Fig. 6b), a swift removal of styrene (82.9%) by the photocatalyst could be discerned in the first 30 min. However, when the UV illumination extended to another 60 min, the decomposition efficiency decreased sharply to 62.6% and then leveled off. This result could be ascribed to the blockage of photocatalytic active sites by stable intermediates on the surface of TiO_2 during the photocatalytic reaction, thereby leading to the deactivation of the photocatalyst [34]. All the prepared TiO_2 sphere multimer photocatalysts in this study showed higher decomposition efficiency for styrene, although a trend similar to P25 was also obtained. For the photocatalyst prepared with the amount of 0.50 g NH_4F added, the decomposition efficiency was 73.0% within 180 min. Increasing the added amount of NH_4F to 0.80 g led to an increase in the decomposition efficiency that peaked at 82.5%. However, further increasing the amount of NH_4F added to 1.20 and 1.50 g decreased the decomposition

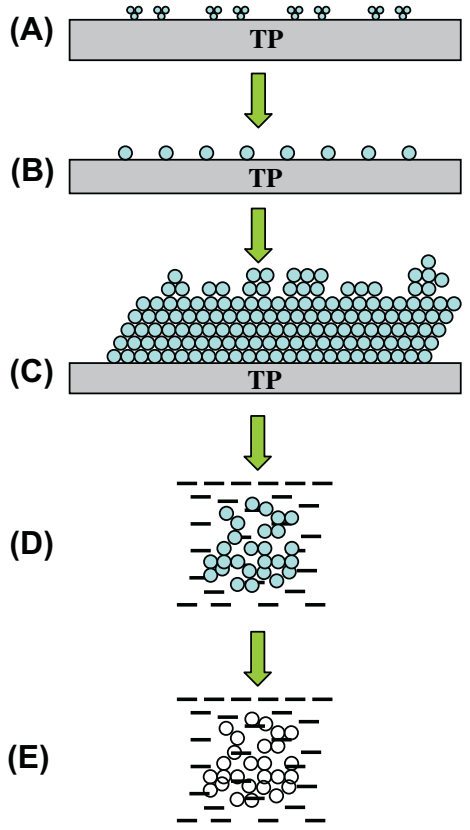

Scheme 1. Schematic illustration of the formation mechanism of the TiO_2 hollow sphere multimers.

efficiency to 67.9% and 65.6%, respectively. The decomposition efficiencies after 180 min of decomposition by different photocatalysts follow the order: P25 (58.5%) < 1.50 g NH_4F (65.6%) < 1.20 g NH_4F (67.9%) < 0.50 g NH_4F (73.0%) < 0.80 g NH_4F (82.5%). All prepared multimer photocatalysts, especially TiO_2 hollow sphere multimers, apparently showed better photocatalytic activity for gaseous styrene than P25 in this study. This enhanced photocatalytic activity may be attributed to the synergistic effects of several factors such as relative crystallinity, specific surface area, band energy and unique hollow multimer structure of this photocatalyst. In the case of specific surface area, TiO_2 hollow sphere multimers do not display the largest specific surface area among the prepared samples. However, it has already been proved that large surface area is not the only decisive factor for the enhancement of the photocatalytic activity of the TiO_2 photocatalyst because TiO_2 with a large surface area is usually accompanied by a large number of crystalline defects, which could act as the centers for the recombination of photogenerated electrons and holes, leading to poor photoactivity of TiO_2 [31,35–37]. Relative crystallinity is also an important factor influencing the photocatalytic activity of TiO_2. As shown in Table 1, the relative anatase crystallinity increases sharply from 1.00 to 1.18 for the samples prepared with the increase of the added amount of NH_4F from 0.50 to 0.80 g. The relative anatase crystallinity then increased slowly to 1.20 and 1.22 for the samples prepared with the added amounts of 1.20 and 1.50 g NH_4F. TiO_2 hollow sphere multimers thus showed the highest photocatalytic activity in this study due to the relatively large surface area, which can efficiently enrich reactant molecules, and good anatase crystallinity, which can reduce the electron and hole recombination. The unique hollow multimer structure can also facilitate the transfer and diffusion of styrene molecules in the catalyst and enhance the light harvesting [21]. Much wider band energy can result in TiO_2 hollow sphere multimers with good redox capability [31]. All these factors combined are responsible for the highest photocatalytic activity of TiO_2 SPMP.

3.6. Formation mechanism

The formation mechanism of TiO_2 SPMP was also investigated by time-dependent evolution experiments for the prepared sample with same added amount of 0.80 g NH_4F. All intermediates were collected at different reaction intervals (2, 6, 12, 22, 36 and 48 h) for detailed investigation. The effect of different reaction times on the morphology of TP with the amount of 0.80 g NH_4F added was carried out initially (Fig. 7) because the reaction on the TP is the first step for the formation of the final powder photocatalyst. After a 2-h reaction, the surface of the TP was rough and full of holes, but no particles were discerned (Fig. 7a). Extending the reaction time to 6 (Fig. 7b) and 12 h (Fig. 7c), the surface of the TP was etched more seriously and became rougher with the formation of more small irregularly shaped particles. When the reaction time was further extended to 22 h (Fig. 3b), the multilayered particles with spherical shapes (accompanied by a few independently multimeric particles) could be observed clearly on the TP surface. Further prolonging the reaction time to 36 h resulted in the formation of more independent multimeric particles with spherical shapes on the TP surface (Fig. 7d). Spheres with the average diameter of approximately 1 μm were formed on the TP surface after 48 h (Fig. 7e).

The powder samples at the different reaction stages (no precipitate was generated in the solution after 2 h of reaction) were also collected and the corresponding XRD, SEM and TEM images are shown in Figs. 8 and 9. Anatase TiO_2 is the only crystalline phase in all powder samples obtained (Fig. 8), while different morphologies are observed at the different reaction intervals. For the powder sample after 6 h of reaction (Fig. 9a), large multimeric particles that are composed of small solid particles with the average diameter of approximately 400 nm are produced (inset of Fig. 9a). By extending the reaction time to 12 h (Fig. 9b), the surface of the particles becomes rough, indicating crystallization of TiO_2 and growth of TiO_2 crystallites. The TEM image (inset of Fig. 9b) reveals that the resultant product is hollow multimers with spherical shapes. However, the multimers obtained are very unstable, and some completely broken particles are clearly discerned. As the reaction time is extended to 22 h, TiO_2 hollow sphere multimers with the average diameter of approximately 400 nm for each sphere are obtained (Fig. 9c), which are then transformed into solid sphere multimers by further extending the reaction time to 36 h (Fig. 9d). This may be due to the collapse of the hollow structures and reconstruction of the particles in the solution. The sample obtained after reaction for 48 h displays a similar morphology to the sample obtained after reaction for 6 h, although the former has larger solid cores (Fig. 9e).

By combining the results shown above, a plausible mechanism for the formation of TiO_2 SPMP was obtained (Scheme 1). First, the TP was etched by generated HF according to the hydrolysis of NH_4F in H_2O solution, and the TiO_2 precursor was formed on the TP surface (Scheme 1A). Subsequently, the TiO_2 precursors were further hydrolyzed to generate TiO_2 particles, which then aggregated to form large TiO_2 particles with spherical shapes due to the self-assembly process (Scheme 1B). Simultaneously, these TiO_2 particles tended to connect with each other to form multimeric particles on the TP surface owing to the existence of the Ti–OH group on the particle surface (Scheme 1C). When more and more particles were formed on the TP, some of them on the top fell into the solution driven by gravity (Scheme 1D). Finally, the hollowing process took place mediated by fluoride to form TiO_2 hollow sphere multimers (Scheme 1E). F^- transfers from the outside

solution to the center of the spheres though the pores between the particles induced the dissolution of TiO_2 to smaller size particles, resulting in an increase of the dissolution rate of the core and the occurrence of hollow spheres [18].

4. Conclusions

TiO_2 (SPMP) was easily fabricated using a low-temperature hydrothermal method by etching TP. Experimental results found that the added amount of NH_4F and hydrothermal time played significant roles in the formation of this photocatalyst, which could only be obtained when 0.80 g NH_4F and TP were added to 40 mL of deionized water, and the hydrothermal time was set at 22 h at a temperature of 120 °C. The decomposition results revealed that all photocatalysts (hollow or solid sphere multimers) prepared by this method showed better photocatalytic activity than Degussa P25 for the photocatalytic decomposition of gaseous styrene, and the TiO_2 SPMP displayed the highest photocatalytic activity due to the synergistic effects of its large surface area, good anatase crystallinity, unique hollow multimer structure and relatively wide band energy. Two major steps were involved in the formation of the TiO_2 hollow sphere multimers: the formation of multimers on the surface of the TP and the hollowing of multimers in the solution.

Acknowledgments

This is contribution No. IS−1679 from GIGCAS. This work was supported by Team Project of Natural Science Foundation of Guangdong Province, China (S2012030006604), the Science and Technology Project of Guangdong Province, China (2012A032300017 and 2011A030700003), the Cooperation Projects of the Chinese Academy of Science with Foshan government (20121071010041).

Appendix A. Supplementary material

Supplementary data associated with this article can be found, in the online version, at http://dx.doi.org/10.1016/j.cej.2013.05.066.

References

[1] M.R. Hoffmann, S.T. Martin, W.Y. Choi, D.W. Bahnemann, Environmental applications of semiconductor photocatalysis, Chem. Rev. 95 (1995) 69–96.
[2] M.A. Fox, M.T. Dulay, Heterogeneous photocatalysis, Chem. Rev. 93 (1993) 341–357.
[3] J.K. Liu, T.C. An, G.Y. Li, N.Z. Bao, G.Y. Sheng, J.M. Fu, Preparation and characterization of highly active mesoporous TiO_2 photocatalysts by hydrothermal synthesis under weak acid conditions, Micropor. Mesopor. Mat. 124 (2009) 197–203.
[4] Y. Li, J.R. Liu, S.Y. Jia, J.W. Guo, J. Zhuo, P. Na, TiO_2 pillared montmorillonite as a photoactive adsorbent of arsenic under UV irradiation, Chem. Eng. J. 191 (2012) 66–74.
[5] J.Y. Chen, G.Y. Li, Z.G. He, T.C. An, Adsorption and degradation of model volatile organic compounds by a combined titania-montmorillonite-silica photocatalyst, J. Hazard. Mater. 190 (2011) 416–423.
[6] J.G. Yu, S.W. Liu, H.G. Yu, Microstructures and photoactivity of mesoporous anatase hollow microspheres fabricated by fluoride-mediated self-transformation, J. Catal. 249 (2007) 59–66.
[7] J.Y. Liao, J.W. He, H.Y. Xu, D.B. Kuang, C.Y. Su, Effect of TiO_2 morphology on photovoltaic performance of dye-sensitized solar cells: nanoparticles, nanofibers, hierarchical spheres and ellipsoid spheres, J. Mater. Chem. 22 (2012) 7910–7918.
[8] W. Jiao, L.Z. Wang, G. Liu, G.Q. Lu, H.M. Cheng, Hollow anatase TiO2 single crystals and mesocrystals with dominant 101 facets for improved photocatalysis activity and tuned reaction preference, ACS Catal. 2 (2012) 1854–1859.
[9] J. Senthilnathan, L. Philip, Photocatalytic degradation of lindane under UV and visible light using N-doped TiO_2, Chem. Eng. J. 161 (2010) 83–92.
[10] R. Asahi, T. Morikawa, T. Ohwaki, K. Aoki, Y. Taga, Visible-light photocatalysis in nitrogen-doped titanium oxides, Science 293 (2001) 269–271.
[11] J.Y. Chen, X.L. Liu, G.Y. Li, X. Nie, T.C. An, S.Q. Zhang, H.J. Zhao, Synthesis and characterization of novel SiO_2 and TiO_2 co-pillared montmorillonite composite for adsorption and photocatalytic degradation of hydrophobic organic pollutants in water, Catal. Today 164 (2011) 364–369.
[12] Y.Z. Li, S.J. Kim, Synthesis and characterization of nano titania particles embedded in mesoporous silica with both high photocatalytic activity and adsorption capability, J. Phys. Chem. B 109 (2005) 12309–12315.
[13] S.M. Zhu, D. Zhang, X.C. Zhang, L. Zhang, X.W. Ma, Y.L. Zhang, M. Cai, Sonochemical incorporation of nanosized TiO_2 inside mesoporous silica with high photocatalytic performance, Micropor. Mesopor. Mat. 126 (2009) 20–25.
[14] D.P. Subagio, M. Srinivasan, M. Lim, T.T. Lim, Photocatalytic degradation of bisphenol-A by nitrogen-doped TiO_2 hollow sphere in a vis-LED photoreactor, Appl. Catal. B – Environ. 95 (2010) 414–422.
[15] A. Fujishima, K. Honda, Electrochemical photolysis of water at a semiconductor electrode, Nature 238 (1972) 37–38.
[16] A. Syoufian, O.H. Satriya, K. Nakashima, Photocatalytic activity of titania hollow spheres: photodecomposition of methylene blue as a target molecule, Catal. Commun. 8 (2007) 755–759.
[17] Z.Y. Liu, D.D. Sun, P. Guo, J.O. Leckie, One-step fabrication and high photocatalytic activity of porous TiO_2 hollow aggregates by using a low-temperature hydrothermal method without templates, Chem. Eur. J. 13 (2007) 1851–1855.
[18] J.G. Yu, J. Zhang, A simple template-free approach to TiO_2 hollow spheres with enhanced photocatalytic activity, Dalton T. 39 (2010) 5860–5867.
[19] Z.Y. Zhong, Y.D. Yin, B. Gates, Y.N. Xia, Preparation of mesoscale hollow spheres of TiO_2 and SnO_2 by templating against crystalline arrays of polystyrene beads, Adv. Mater. 12 (2000) 206–209.
[20] J.N. Liu, G.W. Zhang, W. Ao, K. Yang, S.X. Peng, C. Muller-Goymann, Hollow mesoporous titania microsphere with low shell thickness/diameter ratio and high photocatalysis, Appl. Surf. Sci. 258 (2012) 8083–8089.
[21] J.W. Shi, X. Zong, X. Wu, H.J. Cui, B. Xu, L.Z. Wang, M.L. Fu, Carbon-doped titania hollow spheres with tunable hierarchical macroporous channels and enhanced visible light-induced photocatalytic activity, Chemcatchem 4 (2012) 488–491.
[22] J.J. Xu, M.D. Chen, D.G. Fu, Study on highly visible light active Bi-doped TiO_2 composite hollow sphere, Appl. Surf. Sci. 257 (2011) 7381–7386.
[23] L. Chen, J.H. Li, M.F. Ge, The poisoning effect of alkali metals doping over nano V_2O_5–WO_3/TiO_2 catalysts on selective catalytic reduction of NO_x by NH_3, Chem. Eng. J. 170 (2011) 531–537.
[24] T.Z. Ren, Z.Y. Yuan, B.L. Su, Surfactant-assisted preparation of hollow microspheres of mesoporous TiO_2, Chem. Phys. Lett. 374 (2003) 170–175.
[25] L. Liu, Y.M. Cui, B. Li, X.F. Zhou, W.P. Ding, Study on the surface erosion route to the fabrication of TiO_2 hollow spheres, Appl. Surf. Sci. 256 (2010) 2596–2601.
[26] X. Dong, J. Tao, Y.Y. Li, H. Zhu, Enhanced photoelectrochemical properties of F-containing TiO_2 sphere thin film induced by its novel hierarchical structure, Appl. Surf. Sci. 255 (2009) 7183–7187.
[27] J.Y. Chen, G.Y. Li, Y. Huang, H.M. Zhang, H.J. Zhao, T.C. An, Optimization synthesis of carbon nanotubes-anatase TiO_2 composite photocatalyst by response surface methodology for photocatalytic degradation of gaseous styrene, Appl. Catal. B – Environ. 123–124 (2012) 69–77.
[28] J.C. Yu, J.G. Yu, W.K. Ho, Z.T. Jiang, L.Z. Zhang, Effects of F-doping on the photocatalytic activity and microstructures of nanocrystalline TiO_2 powders, Chem. Mater. 14 (2002) 3808–3816.
[29] M. Kruk, M. Jaroniec, Gas adsorption characterization of ordered organic–inorganic nanocomposite materials, Chem. Mater. 13 (2001) 3169–3183.
[30] Y.J. Xu, Y.B. Zhuang, X.Z. Fu, New insight for enhanced photocatalytic activity of TiO_2 by doping carbon nanotubes: a case study on degradation of benzene and methyl orange, J. Phys. Chem. C 114 (2010) 2669–2676.
[31] M.H. Zhou, J.G. Yu, S.W. Liu, P.C. Zhai, B.B. Huang, Spray-hydrolytic synthesis of highly photoactive mesoporous anatase nanospheres for the photocatalytic degradation of toluene in air, Appl. Catal. B – Environ. 89 (2009) 160–166.
[32] H.G. Yu, J.G. Yu, B. Cheng, M.H. Zhou, Effects of hydrothermal post-treatment on microstructures and morphology of titanate nanoribbons, J. Solid State Chem. 179 (2006) 349–354.
[33] N. Serpone, D. Lawless, R. Khairutdinov, Size effects on the photophysical properties of colloidal anatase TiO_2 particles – size quantization or direct transitions in this indirect semiconductor, J. Phys. Chem. 99 (1995) 16646–16654.
[34] T.C. An, J.Y. Chen, X. Nie, G.Y. Li, H.M. Zhang, X.L. Liu, H.J. Zhao, Synthesis of carbon nanotube-anatase TiO_2 sub-micrometer-sized sphere composite photocatalyst for synergistic degradation of gaseous styrene, ACS Appl. Mat. Interfaces 4 (2012) 5988–5996.
[35] B. Ohtani, Y. Ogawa, S. Nishimoto, Photocatalytic activity of amorphous-anatase mixture of titanium(IV) oxide particles suspended in aqueous solutions, J. Phys. Chem. B 101 (1997) 3746–3752.
[36] K. Tanaka, M.F.V. Capule, T. Hisanaga, Effect of crystallinity of TiO_2 on its photocatalytic action, Chem. Phys. Lett. 187 (1991) 73–76.
[37] J.G. Yu, H.G. Yu, H.T. Guo, M. Li, S. Mann, Spontaneous formation of a tungsten trioxide sphere-in-shell superstructure by chemically induced self-transformation, Small 4 (2008) 87–91.